Phragmoplast of the Green Alga *Spirogyra* Is Functionally Distinct from the Higher Plant Phragmoplast

Heiko Sawitzky and Franz Grolig

Institut für Allgemeine Botanik und Pflanzenphysiologie, Justus-Liebig-Universität, D-35390 Giessen, Federal Republic of Germany

Abstract. Cytokinesis in the green alga *Spirogyra* (Zygnemataceae) is characterized by centripetal growth of a septum, which impinges on a persistent, centrifugally expanding telophase spindle, leading to a phragmoplast-like structure of potential phylogenetic significance (Fowke, L. C., and J. D. Pickett-Heaps. 1969. *J. Phycol.* 5:273–281).

Combining fluorescent tagging of the cytoskeleton in situ and video-enhanced differential interference contrast microscopy of live cells, the process of cytokinesis was investigated with emphasis on cytoskeletal reorganization and concomitant redistribution of organelles. Based on a sequence of cytoskeletal arrangements and the effects of cytoskeletal inhibitors thereon, cytokinetic progression could be divided into three functional stages with respect to the contribution of microfilaments (MFs) and microtubules (MTs): (*1*) Initiation: in early prophase, a cross wall initial was formed independently of MFs and MTs at the presumptive site of wall growth. (*2*) Septum ingrowth: numerous organelles accumulated at the cross wall initial concomitant with reorganization of the extensive peripheral interphase MF array into a distinct circumferential MF array. This array guided the ingrowing septum until it contacted the expanding interzonal MT array. (*3*) Cross wall closure: MFs at the growing edge of the septum coaligned with and extended along the interzonal MTs toward the daughter nuclei. Thus, actin-based transportation of small organelles during this third stage occurred, in part, along a scaffold previously deployed in space by MTs. Displacement of the nuclei-associated interzonal MT array by centrifugation and depolymerization of the phragmoplast-like structure showed that the success of cytokinesis at the third stage depends on the interaction of both MF and MT cytoskeletons. Important features of the phragmoplast-like structure in *Spirogyra* were different from the higher plant phragmoplast: in particular, MFs were responsible for the positioning of organelles at the fusion site, contrary to the proposed role of MTs in the higher plant phragmoplast.

CYTOKINETIC mechanisms partition the cell's constituents between the two resultant daughter cells. In higher plant cells, microtubule (MT)[1] and actin microfilament (MF) cytoskeletons gradually reorganize during mitosis/cytokinesis through a stage-specific sequence of arrays (preprophase band, phragmosome, and phragmoplast), each having a particular function (for reviews see Baskin and Cande, 1990; Staiger and Lloyd, 1991). Despite considerable progress in plant cytoskeleton research, the mechanisms underlying the sequential changes, and the details of the interactions between cytoskeletal elements have remained largely unclear (Wick, 1991). Comparative studies of cytokinesis in related organisms provide a chance to discover the evolutionary sequence leading from a primitive precursor structure to the derived structures, and therefore may help to identify functionally significant elements in the cytokinetic apparatus. The central feature of higher plant cytokinesis is the phragmoplast, which is responsible for initiation and growth of the new cross wall (Gunning, 1982; Wick, 1991).

Based mainly on comparative cytology with emphasis on the type of cytokinesis, a new systematics of the Chlorophyta (green algae) was proposed by Pickett-Heaps and Marchant (1972). In particular, the discovery of a phragmoplastic cell division in some charophycean green algae was a key step forward in our understanding of the relationship between green algae and higher plants (for review see Pickett-Heaps, 1975). This early proposal has received

Parts of this work have been presented at the joint meeting of the Deutsche Gesellschaft für Zellbiologie and the Dutch Society for Cell Biology, Münster, 28 March–1 April 1993, and have appeared in abstract form (1993. *Eur. J. Cell Biol.* [Suppl. 37] 60:43), and at the meeting of the Deutsche Botanische Gesellschaft, Bayreuth, 11–18 September 1994.

Address all correspondence to Dr. F. Grolig, Institut für Allgemeine Botanik und Pflanzenphysiologie, Justus-Liebig-Universität, Senckenbergstraße 17, D-35390 Giessen, FRG. H. Sawitzky's present address is Max-Planck-Institut für Zellbiologie, Rosenhof, D-68526 Ladenburg, FRG.

1. *Abbreviations used in this paper*: CD, cytochalasin D; CWI, cross wall initial; DAPI, 4′,6′-diamidino-2-phenylindole; DIC, differential interference contrast; MF, microfilament; MT, microtubule; NPS, nucleus positioning scaffold; RLP, rhodamine-labeled phalloidin.

substantial support from molecular (Devereux et al., 1990; Surek et al., 1994) and biochemical (De Jesus et al., 1989) data, which establish the close relationship of the zygnematacean green alga to the other charophycean algae. The latter are now widely accepted as being related to the ancestor of the land plant lineage (Mattox and Stewart, 1984; Graham et al., 1991). That a phragmoplast occurs in some, but not all, charophycean green algae (for review see Pickett-Heaps, 1975) suggests that evolution of the phragmoplast took place in the course of establishment of this advanced lineage. One of the organisms of possible phylogenetic significance in the search for rudimentary phragmoplasts is the zygnematacean green alga *Spirogyra*. In contrast to higher plant cells, the new cross wall in *Spirogyra* starts to grow centripetally and then, later apparently forms a phragmoplast-like structure (Fowke and Pickett-Heaps, 1969*b*). Cytokinesis in *Spirogyra* could, therefore, represent an intermediate stage in the evolutionary development of the phragmoplast. The majority of evidence for this phragmoplast-like structure is based on results from electron microscopic studies; however questions concerning the functional significance of the described phragmoplast in vivo remain unanswered (Grolig, 1992).

To investigate cytoskeletal function during cytokinesis in *Spirogyra*, fluorescence and video-enhanced differential interference contrast (DIC) microscopy were used to examine normal and inhibitor-treated *Spirogyra crassa*, a particularly large and translucent species. We were able to correlate organelle redistributions with stage-specific cytoskeletal reorganizations in the cytokinetic process of wall ingrowth. Although the arrays of MTs and MFs finally become integrated during *Spirogyra* cytokinesis, they initially form as separable, recognizably distinct entities. Important features of the cytoskeletal reorganizations in *Spirogyra* are different from those described for the higher plant phragmoplast; therefore, the cytokinetic apparatus in *Spirogyra* appears to be only remotely related to the typical phragmoplast.

Materials and Methods

Plant Material

Spirogyra crassa Kützing was grown in a synthetic medium (Waris, 1953) at 20°C in green light (2,400 lux), under a regime of 14 h light and 10 h darkness. A sufficient increase in synchronized cells was obtained if cells were grown with the same light regime, but at 16°C with increased light intensity (6,000 lux) and an atmosphere of air enriched with 1.1% (vol/vol) CO_2 (Warburg and Krippahl, 1960). The maximum number of mitotic cells (~10%) was found ~6 h after the change of light (both on or off). The cell cycle took 5–6 d under these conditions.

Microscopy

A microscope (Diaplan; Leitz, Wetzlar, FRG) with DIC optics and epifluorescence facilities (75 W Xenon lamp; Ploemopak with filter combinations D, L3 and N2; objectives NPL Fluotar 40, NA 0.7, NPL Fluotar 40, NA 1.32 and NPL Fluotar 100, NA 1.32) was used for the present investigation. Fluorescence micrographs were taken with a camera (MPS-46; Leica Heerbrugg AG, Heerbrugg, Switzerland) using film (TMAX 400-Eastman Kodak Co., Rochester, NY) at 1600 ASA.

Confocal images were obtained using a prototype confocal laser scanning microscope (Leica Laser Technik, Heidelberg, FRG) fitted onto a standard inverted research microscope (IM35; Carl Zeiss Ltd., Oberkochen, FRG; with objective Neofluoar 25, NA 0.8, W-oil). 488 nm of light was generated by an omnichrome krypton/argon ion laser connected to the optical path of the scanning unit via a glass fiber cable. Images were recorded with single direction scan mode and an 8- or 16-fold line scan averaging in a format of 512 × 512 pixels. Data sets of series of optical sections were stored permanently onto an 800-Mb optical cartridge. The set of optical sections was combined in a single image using the rotate option of the image processing package and the processed images were transferred to a slide printing device (Pro-color Premier; Agfa, Leverkusen, FRG) and photographed on 35-mm film (APX100; Agfa).

Video-enhanced Microscopy of Live Cells

Live cells were observed using video-enhanced DIC microscopy to investigate the cytoskeletal dynamics and the effects of cytoskeletal inhibitors. Digitally contrast-enhanced and gray scale–redefined videoframes as obtained in real time using a CCD video camera (DCX-102P; Sony Corp., Park Ridge, NJ) in series with a videodigitizer (Multicon; Leitz) were displayed on a high resolution videomonitor (PVM 1442 QM; Sony). Video sequences were either recorded by a Sony Umatic VO-5800PS, or, for the purpose of eightfold time lapse recording of dynamical aspects, by an AG 6730 (Panasonic, Matsushita Electric Industrial Co., Osaka, Japan). A freeze-frame recorder (RGB version; Polaroid Corp., Cambridge, MA) equipped with a 35-mm camera adaptor was used in the line fill mode for documentation of video frames on Kodak TMAX 100.

Fluorescence Microscopy of MF and MT Arrays, and of the Chromatin Status

For visualization of the actin cytoskeleton, filaments of *S. crassa* were simultaneously fixed and stained with rhodamine-labeled phalloidin ([RLP] 0.16 μmol l^{-1}; Molecular Probes, Eugene, OR) as described (Grolig, 1990), or were stained with FITC-conjugated phalloidin (3.2 μmol l^{-1}; Sigma Chemical Co., Deisenhofen, FRG) for observation in the confocal microscope. MT were visualized by indirect immunofluorescence, using monoclonal anti-β-tubulin (N357; Amersham Buchler, Braunschweig, FRG). Filaments of *S. crassa* were fixed according to Galway and Hardham (1991), gently washed in distilled water, and cracked open in liquid nitrogen for permeabilization. The chromatin status of mitotic cells was visualized using 4′,6′-diamidino-2-phenylindole ([DAPI] 14 μmol l^{-1}; Serva, Heidelberg, FRG), added to cells during fixation (Katsuta et al., 1990). Cells were mounted in Mowiol 4-88 (Calbiochem, Novabiochem, Bad-Soden, FRG) with 0.1% (wt/vol) *p*-phenylenediamine (Grolig et al., 1988).

Functional Analysis by Cytoskeletal Inhibitors

Functional aspects of the cytoskeletal arrays during cytokinesis were investigated by the application of cytochalasin D ([CD] 10 μg ml^{-1}; stock of 1 mg ml^{-1} in DMSO (Sigma Chemical Co., Taufkirchen, FRG) to depolymerize MFs (Schliwa, 1982), and of oryzaline (10^{-6} mol l^{-1}; stock of 25 mmol l^{-1} in acetone, kindly provided by Eli Lilly, Bad Homburg, FRG) to depolymerize MTs (Morejohn et al., 1987). Both inhibitors were applied in culture medium under the microscope.

Cell Centrifugation

To test the dependence of cytokinetic progression on the presence of mitotic structures, these components were displaced by centrifugation. After selection of distinct cytokinetic stages, single filaments of *S. crassa* were sandwiched between two slabs of agar (3% wt/vol; Fujii et al., 1978) and wedged into a centrifuge tube. The filaments were centrifuged in longitudinal direction (600 *g*, 20 min) in a swing-out rotor (Mikro-Rapid, Hettich, Tuttlingen, FRG), and then transferred to culture medium.

Results

Overlap of Mitosis and Cytokinesis

Cytokinesis in *S. crassa* took more than nine hours from initial ingrowth of the septum to cross wall completion, and started shortly after beginning of the mitotic prophase. A temporal and spatial overlap of mitosis and cytokinesis led to a sequence of characteristic cytokinetic formations,

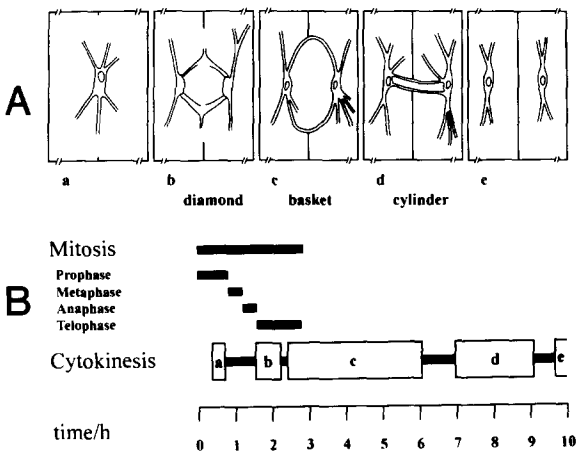

Figure 1. Schematic illustration of the spatial and temporal integration of mitosis and cytokinesis in *S. crassa*. (*A*) Sequence of sketches, depicting characteristic stages during cytokinesis. (*a*) Initiation of cytokinesis in mid-prophase, characterized by appearence of a CWI and an accumulation of organelles at the division site. (*b*) The diamond stage resulting from lateral expansion of the persistent telophase spindle. (*c*) After making contact with the ingrowing cross wall, the diamond structure transforms into the basket structure. (*d*) Upon further ingrowth of the cross wall, the basket structure transforms into the cylinder structure. (*e*) Two daughter cells on completion of cytokinesis. (*B*) Diagram illustrating the duration of mitosis in *S. crassa* (~9.5 h) and its overlap with cytokinesis. The average time of each mitotic stage is: prophase, 50 min; metaphase, 20 min; anaphase, 25 min; telophase, 70 min. The duration of the specific cytokinetic stages shown in *A* is outlined in the time bar of cytokinesis.

which are depicted schematically in Fig. 1 *A*. The length of the mitotic and cytokinetic phases are outlined in Fig. 1 *B*.

Dynamics of Cytokinesis: Rearrangement of MF and MT Arrays

Interphase. Throughout interphase, the nucleus of *S. crassa* was held at the cell center by a scaffold of rigid stalks (Fig. 2 *A*) named the nucleus positioning scaffold (NPS). The stalks of the NPS radiated from the rim of the lens-shaped nucleus towards the peripheral cytoplasm and terminated after occasional branching on the spiral chloroplast bands. No specific premitotic events were detected by video-enhanced DIC microscopy.

The interphase actin cytoskeleton comprised of MFs running along the stalks of the NPS (Fig. 3 *A*) and a variable and extensive system of MF bundles in the cell periphery (Fig. 3 *B*). The lenticular nucleus was covered by unbundled F-actin.

MTs were detectable in the stalks of the NPS extending from the nuclear rim (Fig. 4, *A* and *B*) and on the nuclear surface. Cortical, parallel MTs were oriented perpendicular to the cell's long axis (not shown). No structure reminiscent of a preprophase band could be detected (Fig. 4 *C*).

Onset of Mitosis Up to Anaphase and Initiation of Cytokinesis. The first indication of the onset of mitosis was a swelling of the nucleus at early prophase (Fig. 2 *B*). A few minutes later, a tiny cross wall initial (CWI) appeared in the cell cortex at the future division plane (Fig. 2 *I*). At that time, small organelles accumulated at the CWI, marking the beginning of centripetal septum ingrowth. The nucleus swelled, becoming cylindrical in shape, and elongated twofold into a barrel-shaped metaphase spindle (Fig. 2 *C*). Chromosome segregation correlated very closely with segregation of the spindle poles: the distance between chromosomes and spindle poles remained constant throughout most of anaphase, until a slight decrease was observed in late anaphase. Highly refractile strands of the interzonal spindle (Fig. 2 *F*) sometimes persisted into late telophase. After the chromosomes had gathered at the poles, the interzonal spindle extended further towards the cell periphery.

At mid-prophase, the extended interphase system of MF bundles vanished, and concomitantly, a narrow but prominent accumulation of MFs appeared at the prospective division site (Fig. 3 *C*). In the resulting circumferential band, short MF bundles ran at different angles toward the CWI, i.e., were not orientated in parallel to the division plane. The density of MFs within this array continued to increase up to the anaphase/telophase transition (Fig. 3 *G*). Concomitant to rearrangement of the peripheral actin cytoskeleton, the amount of perinuclear F-actin increased, reaching a maximum at the transition from prophase to metaphase. Weak RLP fluorescence was also detected within the nucleus (Fig. 3 *D*). The mitotic chromatin status could be readily detected by DAPI staining of the nuclear DNA in situ (Fig. 3, *L–O*), and related to the structural changes of the MF and the MT cytoskeleton.

MT-related fluorescence around the nucleus increased at the onset of cell division, but weakened in the stalks of the NPS (Fig. 4 *C*). At metaphase, the mitotic spindle appeared as a fibrillar barrel (Fig. 4 *D*). Cortical MTs persisted throughout mitosis, though at lower density. No MTs were found colocalized with the circumferential band of MFs at the septum edge.

Anaphase/Telophase: Formation of the Diamond Structure. From early anaphase on, numerous cytoplasmic threads grew from the former spindle poles in all directions into the vacuolar space (Fig. 2 *E*). These spikes exhibited phases of erratic growth and shrinkage (Fig. 2, *G* and *H*). By the end of anaphase, a diamondlike structure had formed from the persistent spindle and the outgrowing spikes. The antiparallel elements of the diamond structure appeared to become interconnected in the division plane, as indicated by continous striation (Fig. 2 *F*). The tips of the diamond structure were located at the former spindle poles enclosing the reforming nuclei (Fig. 5 *A*). During all mitotic stages, cytoplasmic strands were seen along the potential division site spanning the cytoplasm between the dividing nucleus and cell periphery (Fig. 2 *D*).

The weak RLP fluorescence detected within the nucleus became fibrillar during segregation of the chromosomes (Fig. 3 *E*). At the beginning of telophase, only very weak RLP fluorescence was present in the nuclear region and in the diamond structure. In the peripheral cytoplasm, F-actin was found only in the then very prominent circumferential band (Fig. 3 *G*). A projection of a series of optical sections obtained by confocal microscopy (Fig. 3 *F*) gives an impression of the arrangement of such a telophase scaffold.

With continuing separation of the chromosomes (Fig. 4, *E* and *F*), numerous interzonal MTs elongated from the

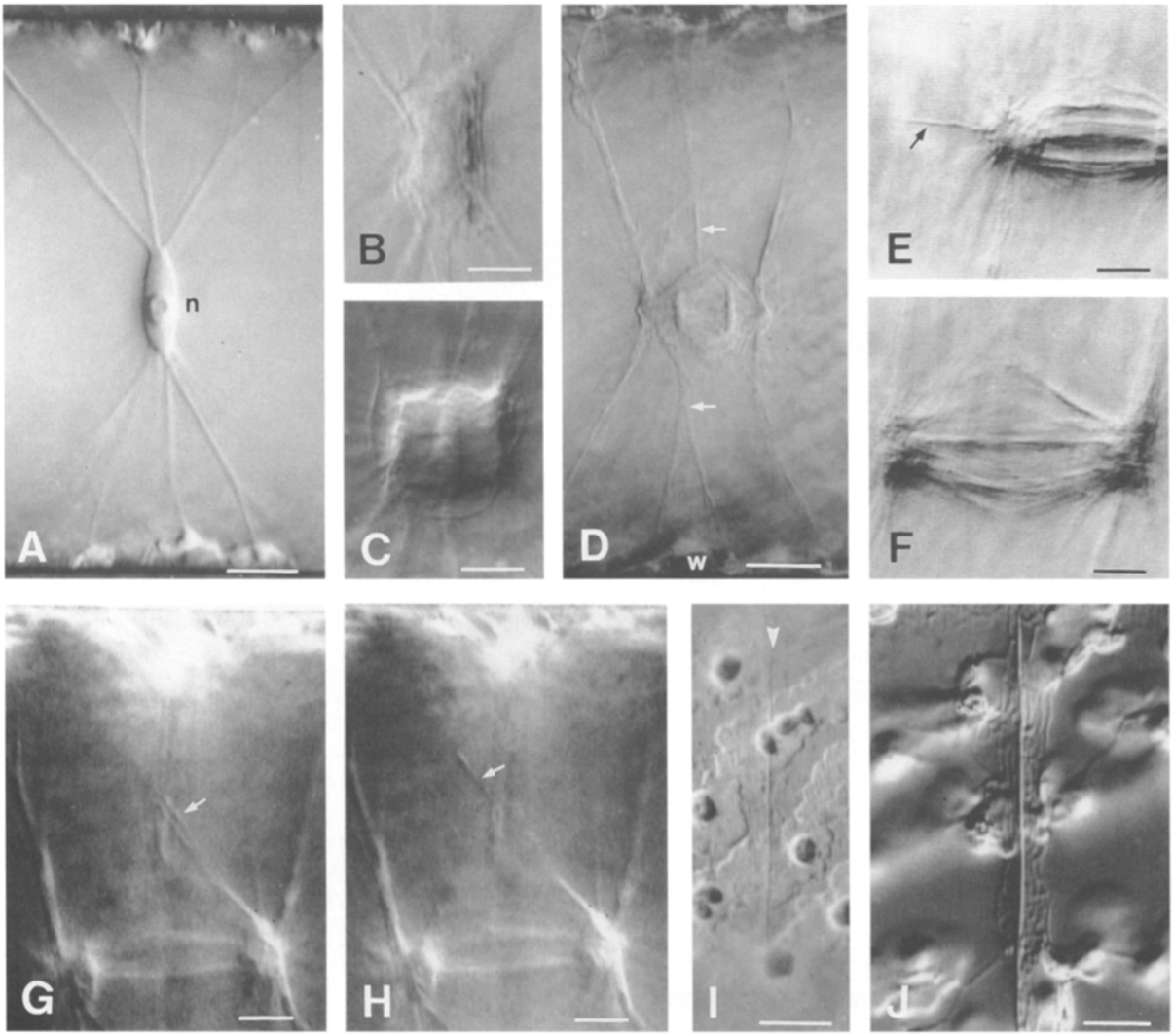

Figure 2. Video-enhanced DIC microscopy of live cells of *S. crassa.* (*A*) Interphase. Midplane view showing the nucleus positioning scaffold which connects the lens-shaped nucleus (*n*; with nucleolus inside) to the cell periphery. (*B–F*) Progression through mitotic stages, midplane views. Note the enormous elongation of the spindle. (*B*) Prophase. A swelling nucleus surrounded by an increased number of organelles. (*C*) Metaphase. Mitotic spindle of barrel shape with central metaphase plate and accumulations of organelles at the spindle poles. (*D*) Mid-anaphase with two chromatin plates. The spindle poles become pointed and a diamond structure results from expansion of the interzone towards the cell periphery. Cytoplasmic strands (*small arrows*) in division plane connect the nucleus to the cell periphery throughout mitosis. *w*; ingrowing cross wall. (*E*) Detail of late anaphase. Note cytoplasmic thread (*arrow*) growing out from the spindle pole. (*F*) Early telophase. Interzone with prominent spindle fibres; chromosomes have approached the spindle poles. (*G–H*) Detail of the diamond structure at early telophase, showing outgrowth of a cytoplasmic thread (*arrow*) at an interval of 30 s. (*I*) CWI (*arrowhead*) in the periphery of a prophase cell. (*J*) Anaphase. Accumulation of organelles at the edge of the ingrowing septum. Bars, 10 μm. In micrographs *A*, *D*, and *I*, 20 μm.

Figure 3. (*A–K*) Visualization of the actin cytoskeleton in fixed cells of *S. crassa* by RLP or by FITC-phalloidin (*F* and *J*). (*A–B*) Interphase. (*A*) Mid-plane view. F-actin encases the nucleus (*n*), and is found in the stalks of the NPS. (*B*) The peripheral cytoplasm contains numerous MF bundles without preferential orientation. (*C*) Prophase. A thin circumferential band of F-actin has formed in the cell periphery. (*D*) Prometaphase. Mid-plane view. The nucleus (*n*) is brightly stained with RLP. Increase of RLP fluorescence in the cell periphery indicates further accumulation of MFs in the circumferential band. (*E*) Late anaphase. Mid-plane view. The intensity of staining in the peripheral band reaches its maximum. Some stain in the spindle is preferentially orientated along the spindle axis. Arrows denote position of chromosomes. (*F–G*) Early telophase. (*F*) Telophase configuration observed by confocal laser–scanning microscopy. Projection of a series of optical sections in a single image. The division plane shows the nuclear region with diffuse FITC–phalloidin fluorescence of decreased intensity. The reforming nuclei (*n*) show slightly increased FITC–phalloidin fluorescence. The circumferential actin band at the ingrowing cross wall (*w*) is brightly stained. (*G*) Detail of the prominent circumferential band of F-actin. MFs run at different angles to the division plane. (*H*) Late telophase. Midplane view of MF distribution in the basket structure. Formation of MF bundles (*arrow*), connecting the intensely stained daughter nuclei (*n*). Loss of tension in the basket and approach of nuclei is caused by fixation. (*I*) Mid-cytokinesis; detail of circumferential actin band just before transformation of the basket structure into the cylinder structure.

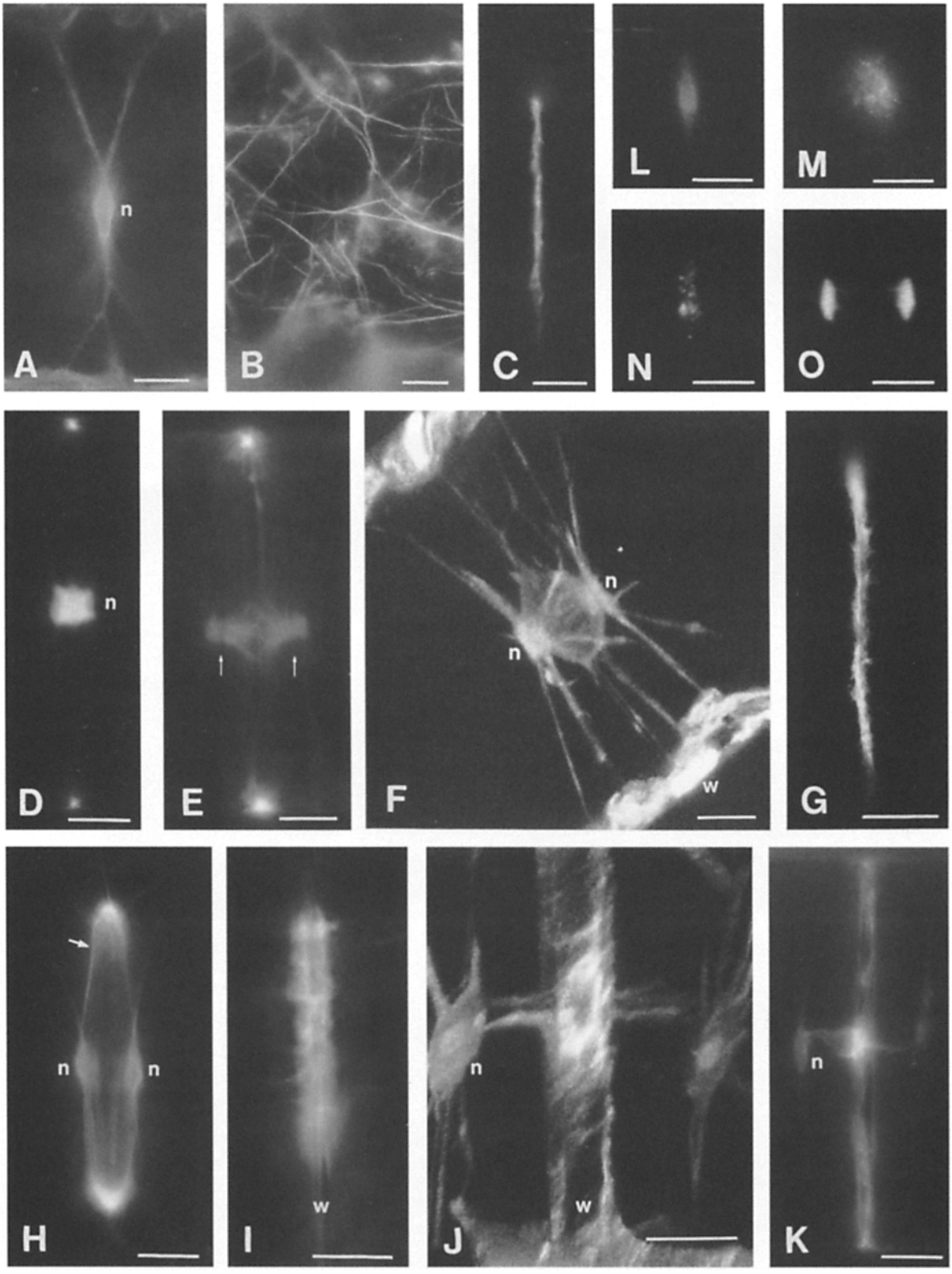

The orientation of MF bundles is parallel to the connecting strands. *w*; cross wall. (*J*) Cylinder structure observed by confocal microscopy. Projection of a series of optical sections shows persistence of a prominent MF accumulation at the edge of the closing septum. MFs encase the nuclei (*n*), and connect them with the septum edge. Diffuse FITC–phalloidin fluorescence is seen on both sides of the new cross wall (*w*). (*K*) Late cytokinesis. Midplane view shows RLP-stained strands connecting the F-actin encased nuclei (*n*) and the septum and prominent RLP staining on the new cross wall. (*L–O*) Staining of DNA with DAPI. (*L*) Interphase, compare Fig. 3 *A*. (*M*) Prophase, compare Fig. 4 *C*, showing condensing chromatin. (*N*) Prometaphase, compare Fig. 3 *D*, showing chromatin arranging to a metaphase plate. (*O*) Anaphase, compare Figs. 3 *E* and 4 *F*. Segregation of chromosomes, with some chromosomes lagging behind. Bars, 20 μm. In micrographs *B*, *I*, *J*, and *L–O*, 10 μm.

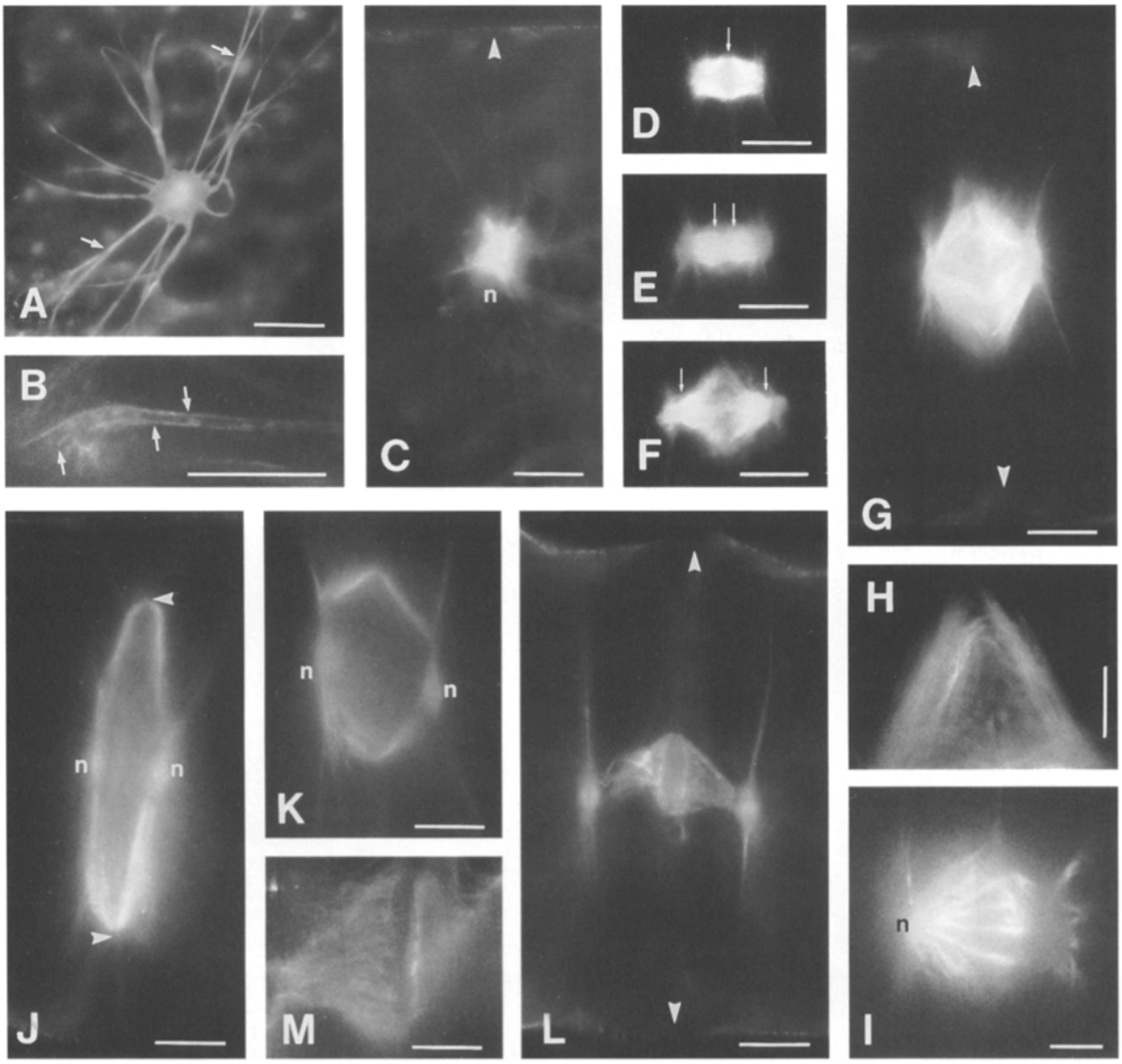

Figure 4. Visualization of MTs in fixed cells of *S. crassa* by indirect immunofluorescence. (*A–B*) Interphase. (*A*) Front view of a nucleus positioning scaffold. Bundles of MTs are found in the stalks; note branching points (*arrows*). Fixation-derived fluorescence of the nucleolus blurs the MT-related fluorescence around the nucleus. (*B*) Detail of the MTs (*arrows*) of a stalk at its nuclear insertion site. (*C*) Midplane view at early prophase. MT fluorescence has increased at the swollen nucleus (*n*). MTs occur in the cortex (*arrowhead*), but no preprophase band is found. (*D*) Metaphase. Midplane view of the barrel-shaped mitotic spindle. Position of chromosomes is indicated by arrow. (*E–F*) Midplane views of anaphase. Position of chromosomes (*arrows*). (*E*) Early anaphase. (*F*) Late anaphase, interzonal MTs widening at the equator, early diamond structure. (*G–I*) Early telophase. (*G*) Midplane view of the brightly stained diamond structure. No MTs are found in the circumferential band at the septum edge (*arrowheads*). (*H*) Detail of the diamond structure at the periphery. (*I*) Top view of the diamond structure with prominent MT bundles centering on the spindle pole. *n* marks the position of the reforming nucleus. (*J*) Late telophase. Midplane view of the basket structure with thick MT bundles connecting the nuclei to the septum edge (*arrowheads*). Loss of tension and approach of the nuclei (*n*) is due to fixation. (*K*) Late basket structure. Midplane view of MTs connecting the nuclei (*n*) to the septum edge. (*L–M*) Cylinder structure. (*L*) Midplane view; numerous MTs connecting the nuclei to the septum edge. Increased interphase-like MT-related fluorescence in the cell cortex, but no MTs detectable adjacent to the new cross wall (*arrowheads*). (*M*) Detail of a cylinder structure with numerous longitudinal MTs. No thick MT bundles are visible. Bars, 20 μm. In detail micrographs *B*, *H*, *I*, and *M*, 10 μm.

spindle poles causing the persisting spindle to bulge out towards the cell periphery, leading to a diamond structure at the beginning of telophase (Fig. 4, *G–I*). Numerous MTs (Fig. 4, *G–H*) and some MT bundles (Fig. 4 *I*) could be discerned.

Mid-Cytokinesis: Formation of the Basket Structure. The diamond structure expanded continously, approaching the ingrowing septum. Once contact had been established, the fine strands drawing from the daughter nuclei to the ingrowing septum appeared to condense into fewer, but thicker strands, transforming the diamond structure into a basketlike structure (Fig. 5, *B* and *C*). While the daughter nuclei at that time stayed in position, the strands connecting to the ingrowing septum continued to elongate up to late telophase and began to bend as if under tension.

The distribution of MFs changed during telophase. On

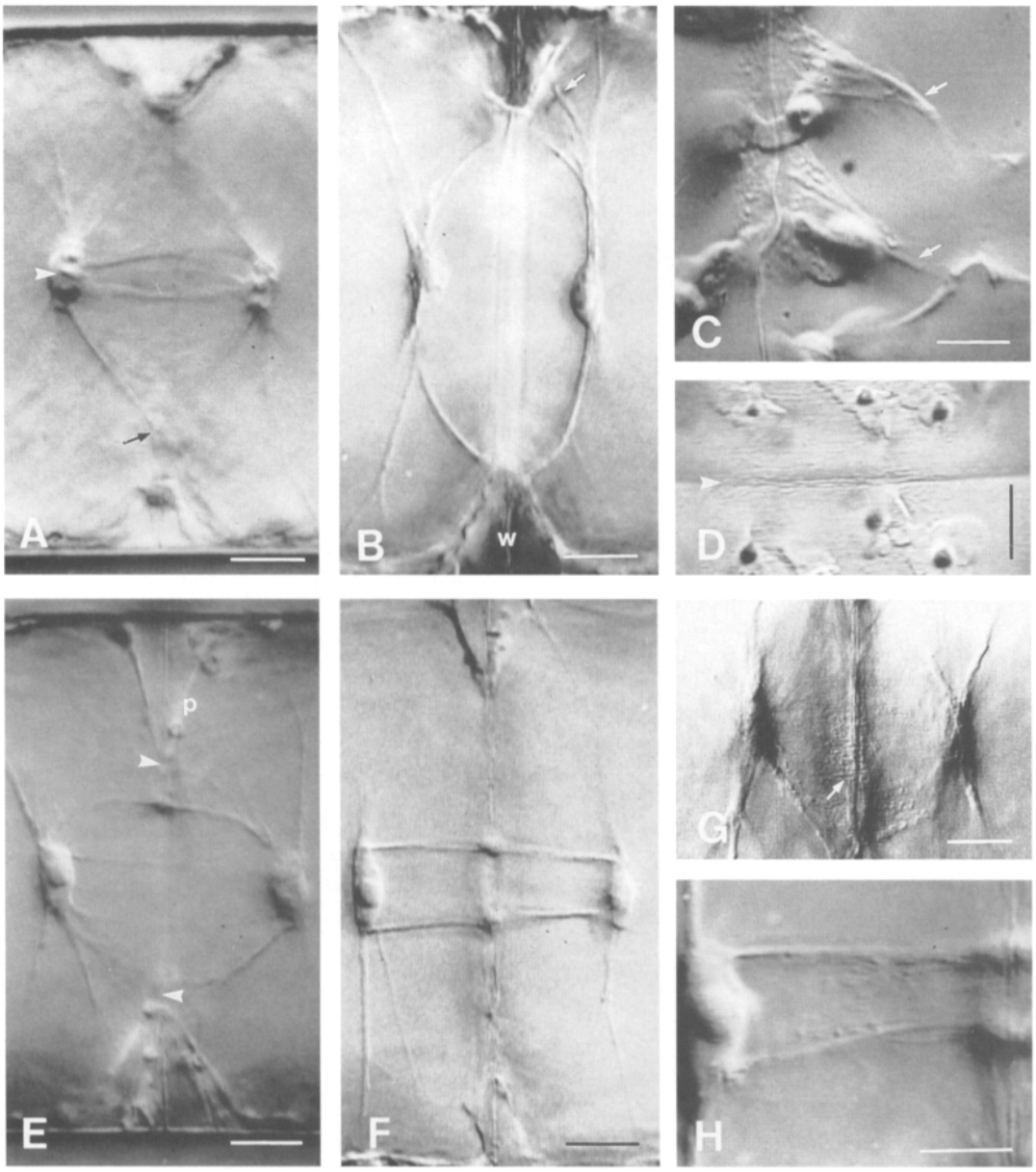

Figure 5. Video-enhanced DIC micrographs of live cytokinetic cells of *S. crassa.* (*A*) Mid-telophase with fully developed diamond structure, reaching to the edge of the ingrowing septum (*arrow*). In this stage the nucleoli are reforming (*arrowhead*). (*B–D*) Basket structure at late telophase. (*B*) Midplane view showing daughter nuclei with reformed nucleoli. Prominent, bent bundles connect nuclei and septum edge. Note bundles (*arrow*) connecting nucleus and chloroplast nearby the septum. *w*; cross wall. (*C*) Detail of the basket structure at septum edge with organelle accumulation spreading out over the thick bundles of the basket (*arrows*). Chloroplast bands are drawn into the cell and extend over the septum edge. (*D*) Peripheral view, showing the new cross wall (*arrowhead*) central in a large chloroplast-free region. (*E*) Late basket structure, transient to cylinder structure. Midplane focus of a smaller basket. Chloroplast bands (*p*) are severed and stay behind (*arrowheads*) the growing edge of the cross wall. (*F*) Midplane view at late cytokinesis shows the cytoplasmic cylinder that connects the daughter nuclei to the new cross wall. The central gap of the cross wall indicates further centripetal growth. (*G*) Detail of the transition stage from basket structure to cylinder structure. Fine striated cytoplasm from now on connects the whole septum to the nuclei, with many, nonmoving organelles (*arrow*) aligned along the axis. (*H*) Detail of the cylinder structure at septum edge shows fine striated cytoplasm without thick bundles. Bars, 20 μm. In detail micrographs *C*, *D*, and *H*, 10 μm.

formation of the basket structure, MFs gathered to form bundles extending between the newly formed nuclei and the rim of the septum (Fig. 3 *H*). The nuclei again were covered by bright RLP fluorescence as in interphase, and also the stalks of the remaining (old) part of the NPS showed increase of RLP fluorescence. Although this structure collapsed upon aldehyde fixation, strong signals of the fluorescent tags for F-actin (Fig. 3 *H*) and MTs (Fig. 4 *J*) were detected.

The MT array of the diamond structure with numerous MTs and some MT bundles persisted up to the basket stage in late telophase, where the bundling of the MTs increased (Fig. 4 *J*).

Completion of Cytokinesis: Formation of the Cylinder Structure. Concomitant with ongoing ingrowth of the septum, the basket structure steadily decreased in diameter (Fig. 5 *E*), finally attaining a cylindrical structure of further decreasing diameter (Fig. 5 *F*). During this transformation,

the rather thick strands of the basket structure (Fig. 5 *C*) were substituted by numerous thinner strands (Fig. 5 *G*) which were arranged strictly transverse to the ingrowing septum (Fig. 5 *H*).

After the basket structure had formed, the variable orientation of the MFs attached to the rim of the septum changed into a defined orientation strictly perpendicular to the plane of the septum (Fig. 3 *I*). The projection of a set of optical sections obtained by confocal microscopy of the subsequent cylinder structure (Fig. 3 *J*) shows a still distinct, but broadened ring of FITC–phalloidin fluorescence around the closing gap in the new cross wall. Increased MF-related fluorescence was observed at the ingrown cross wall and around the already interphase-shaped nuclei. The reestablishing interphase system of extended MF bundles in the peripheral cytoplasm appeared especially dense at the new cross wall for hours (Fig. 3, *J* and *K*).

During transformation into the cylinder structure, the thicker MT bundles of the late basket structure (Fig. 4 *K*) were progressively substituted by thinner MT bundles, which then extended strictly perpendicular from the rim of the septum towards the nuclei (Fig. 4 *M*). The fluorescence of the cortical MTs gradually increased again, but adjacent to the newly ingrown wall (Fig. 4 *L*), MTs transiently disappeared.

Organelle Redistributions

During interphase, numerous small vesicles, mitochondria, and less abundant ER-like membrane tubules were distributed throughout the peripheral cytoplasm and along the NPS. This distribution changed profoundly upon onset of mitosis, when the organelles became concentrated at specific, active sites. The schemes in Fig. 6 provide a qualitative survey of the extent and the direction of net translocation, and of the distribution of organelles at typical stages of cytokinesis.

At the beginning of mitosis, most of these organelles accumulated at the division site marked by the CWI, and in the perinuclear cytoplasm (Fig. 2, *B* and *C*); otherwise organelle transportation almost completely subsided. The number of organelles accumulated at the edge of the growing septum and reached its maximum at anaphase (Figs. 2 *J* and 6 *B*), with very few remaining in the peripheral cytoplasm. Meanwhile, those in the perinuclear cytoplasm became focused at the spindle poles (Fig. 2 *E*). Both populations revealed a distinct and intense short-range motility. Upon contact of the ingrowing septum with the expanding diamond structure, the organelle accumulation at the edge of the septum underwent a significant rearrangement and change in motility (Fig. 6 *C*); ER-like membrane tubules coaligned with the stalks of the basket structure perpendicular to the division plane (Fig. 5 *C*). Together with numerous vesicles, the membrane tubules dispersed over the basket (Fig. 5 *G*), but remained positioned, i.e., without any further substantial translocation, during initial transformation of the basket into the cylinder structure (Fig. 5 *H*). When septum ingrowth approached completion, time-lapse recording revealed increasing net translocation of organelles from the closing septum towards the nuclei, first along the strands of the cylindrical structure (Fig. 6 *D*), later along a central residual cytoplasmic strand. At the same time, the interphase translocation system reestablished, initially along the stalks of the reforming NPS, and later in the cell periphery.

During primary ingrowth of the septum, the chloroplast bands were drawn into the cell, stretching over the septum edge from one cell half into the other (Fig. 5 *A*). Soon after the diamond structure associated with the growing septum, the chloroplast bands became severed, but stayed attached to the sides of the ongrowing septum (Fig. 5, *D* and *E*) until long after completion of cytokinesis.

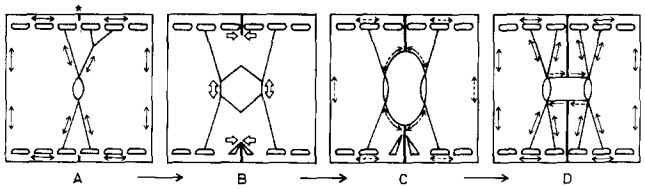

Figure 6. Sketches of optical sections of *S. crassa* summarizing organelle translocation activities in various regions of the cell during the cell cycle. Tip of arrow indicates direction, length of arrow relative range of organelle translocation; thickness of arrow indicates relative abundance of organelles in the respective region. (*A*) interphase, (*B*) diamond structure (late anaphase), (*C*) basket structure (late telophase), (*D*) cylinder structure (late cytokinesis). *, site of CWI; chloroplast bands are indicated in the peripheral cytoplasm.

Cytoskeletal Inhibitors

The functional significance and interdependence of MTs and MFs for the maintainance and dynamic transformation of specific cytoskeletal arrays and for the redistribution of organelles during cytokinesis could be readily tested by application of oryzalin and CD.

Effects of Oryzalin. Two phases of cytokinesis could be distinguished with respect to their sensitivity to oryzalin: (*1*) Both formation of the CWI and the first phase of ingrowth after the accumulation of organelles in the division plane, proceeded in the presence of oryzalin until the septum closed up to slightly more than half of the cell radius (Fig. 7, *A* and *B*). No mitotic spindle appeared if oryzalin was applied during prophase. Upon prolonged application (>1 h), the nucleus left the central position and moved towards the septum (Fig. 7 *B*). Finally, the accumulation of organelles at the growing septum vanished, and septum growth stopped (Fig. 7, *C* vs. *D*). If oryzalin was applied at meta- or anaphase, the spindle broke down within seconds and the separated sets of chromosomes congregated. The numerous stiff cytoplasmic threads, growing out during anaphase from the former spindle poles into vacuolar space, disappeared. The diamond (Fig. 7 *E*) and basket structures collapsed after application of oryzalin; in both cases the daughter nuclei approached each other. (*2*) If oryzalin was applied during transformation of the basket to the cylinder structure or at a later stage, ingrowth ceased within minutes. The highly ordered cylinder structure rapidly collapsed into a single, thick cytoplasmic strand (Fig. 7, *F–H*).

Effects of CD. While the CWI formed unimpaired in the presence of 10 $\mu g/ml^{-1}$ CD given up to 3 h before prophase (Fig. 8 *D*), the accumulation of motile organelles at the

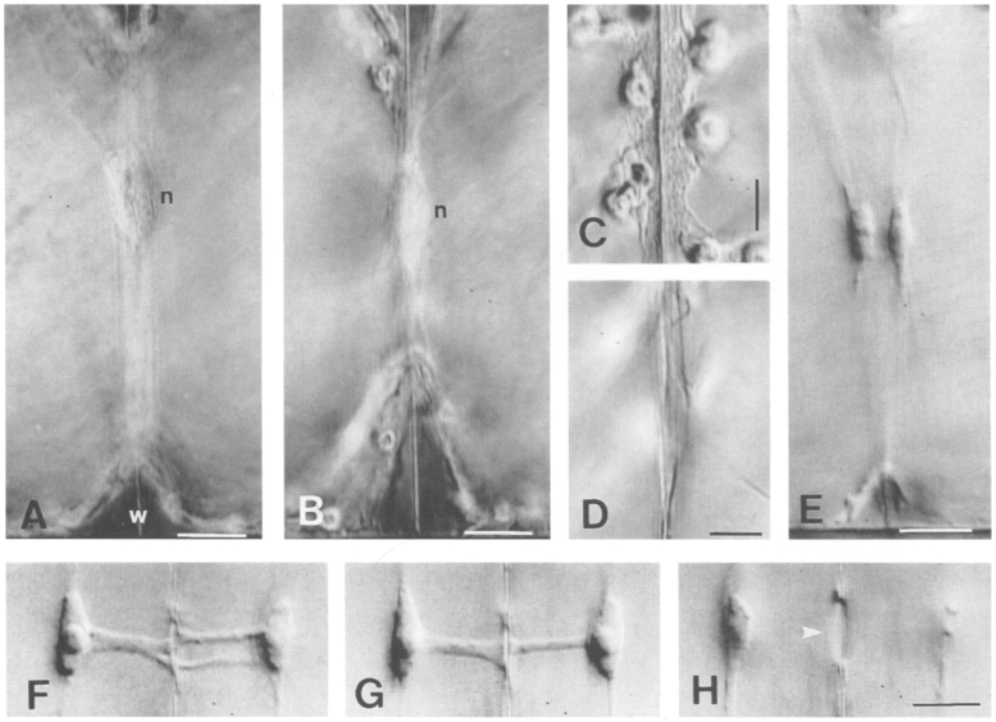

Figure 7. Video-enhanced DIC micrographs of live cells of *S. crassa*, treated with 1 μmol l^{-1} oryzalin. (*A–D*) Rapid breakdown of the nucleus positioning scaffold after treatment at early prophase. (*A*) Midplane view, after 45 min of treatment. The nucleus (*n*) resides in the cell center. No mitotic spindle is formed; cross wall (*w*) ingrowth is undisturbed. (B) Same cell, focus on the lower septum edge after 1.5 h of treatment. The nucleus (*n*) has moved close to the septum edge. Cross wall ingrowth has stopped at about half the cell radius. (*C*) Same cell, focus on the upper septum edge after 45 min of treatment. Detail of organelle accumulation, comparable to untreated cells. (*D*) Same cell, focus on the upper septum edge after 1.5 h of treatment. Disappearance of organelle accumulation correlates with ceased ingrowth. (*E*) Midplane view 30 min after start of treatment at early telophase. Breakdown of the diamond structure results in approach of the daughter nuclei. (*F–H*) Upon treatment of the cylinder structure, the distance between the daughter nuclei keeps approximately constant. (*F*) Midplane view. After 15 min of treatment, the cylinder collapses into a few thick strands. (*G–H*) Same cell after 30 min of treatment. (*G*) Focus on septum edge shows a single, thick strand of cytoplasm with organelles moving along. (*H*) Midplane view shows the gap in the new cross wall (*arrowhead*); ingrowth has stopped. Bars, 20 um. In micrographs *C* and *D*, 10 um.

CWI, and the ingrowth of the septum were completely inhibited. The later the drug was applied, the smaller the effect of CD on the accumulation process. If CD was applied after the basket structure had formed, it only caused delay of further septum ingrowth (not shown); this effect also decreased the later the drug was applied. The formation of organelle accumulations, which behaved like ameboid pockets of cytoplasm, was observed in the presence of CD during all stages of cell division. Such pockets were found in particular on the cytokinetic NPS, at branching points of the basket structure, and close to the nuclei. However, mitosis proceeded unimpeded in the presence of CD (Fig. 8, *A* and *B*), resulting in binucleated cells. Though both nuclei were supported by a complete NPS (Fig. 8 *C*), often they were not positioned precisely in the center of the cell.

Cell Centrifugation

During longitudinal centrifugation, the daughter nuclei with their associated scaffolds linked to the chloroplasts were dislodged into the centrifugal part of the cell (Fig. 9 *A*). In *S. crassa*, two stages of cytokinesis could be distinguished on the basis of differential effects of centrifugation. In the early stage of septum ingrowth, before the basket structure had formed, growth of the septum proceeded normally, but ceased a few hours after centrifugation. The cross wall (Fig. 9 *D*) was not completed, although the organelle accumulation at the septum edge (Fig. 9 *B*) and the direction of ingrowth (e.g., Fig. 9 *D*) appeared undisturbed. When cells were centrifuged after the basket structure had already formed, the septum grew almost to completion, but the organelle accumulation at the septum edge changed (Fig. 9 *E*) and major disturbances in growth direction led to gaps in the new cross wall (Fig. 9 *F*). No redistribution of organelles from the septum edge into the daughter cells was observed after centrifugation.

Discussion

Three Functionally Distinct Stages of Cytokinesis

In *S. crassa*, susceptibility to cytoskeletal inhibitors during cytokinesis could be divided into three stages (Fig. 10): (*1*) formation of the CWI was neither inhibited by CD, nor oryzalin; (*2*) primary ingrowth of the septum was impeded by CD, but remained unimpaired by oryzalin; (*3*) closure of the new cross wall was disturbed by both drugs.

The onset of cell wall initiation in *Spirogyra* in the presence of cytoskeletal inhibitors (applied a few hours before prophase) suggests that construction of the CWI occurs independent of the MF and MT cytoskeletons. All factors needed for cross wall initiation, i.e., positioning factors and the growth machinery, seem to be present at the division site before detectable mitotic changes of the cytoskeletal arrays (stage 1). In the absence of an active transport system, it is possible that cell-wall material reaches active growth sites by diffusion, resulting in construction of the tiny CWI. In contrast, centripetal ingrowth from the CWI is inhibited by CD, and therefore apparently depends on

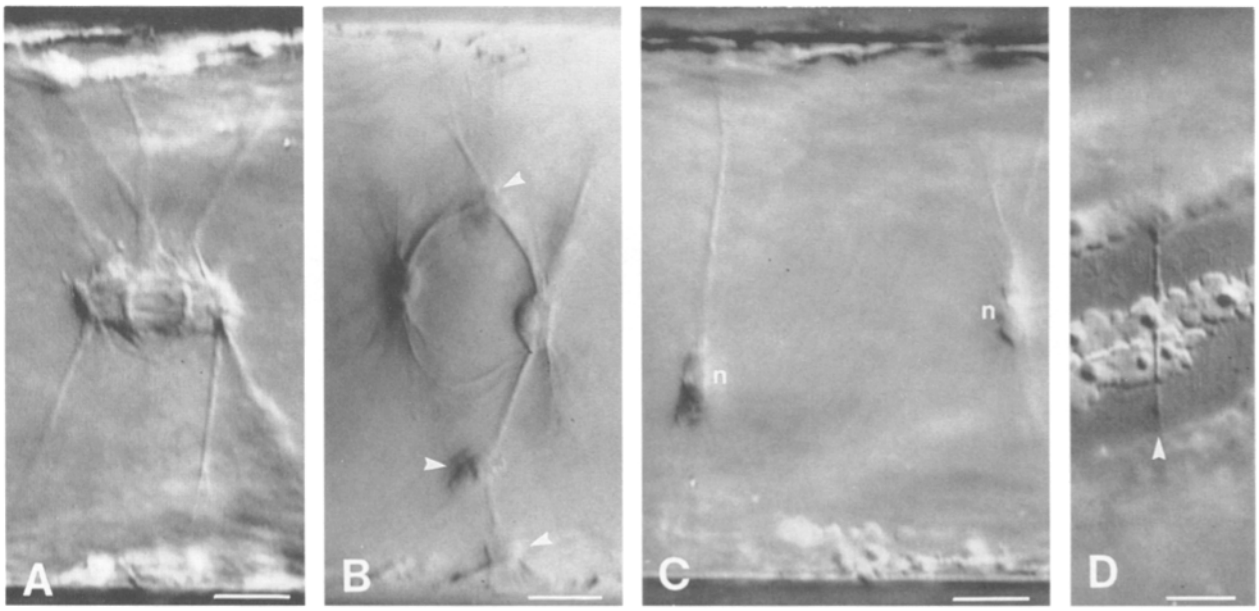

Figure 8. (*A–D*) Micrographs of live *S. crassa*, treated with 10 μg ml^{-1} CD before mitosis and observed by video-enhanced DIC microscopy. The cell entered mitosis 1 h after the commencement of treatment. (*A*) Mid-anaphase nucleus, 2.5 h after treatment with CD, showing segregating chromosomes. (*B*) Formation of the basket structure at telophase without ingrowth of and contact with the septum. Very thick accumulations of cytoplasm (*arrowheads*) in division plane. (*C–D*) Same cell as in (*A*), after 24 h of treatment. (*C*) Midplane view showing two lenticular interphase nuclei (*n*), each positioned somewhat excentrically. A new cross wall has not formed. (*D*) Only the CWI (*arrowhead*) is evident in the cortex. Bars, 20 μm.

an active supply of the wall-growth machinery along the division plane via a functional actin cytoskeleton.

In the last two stages of cytokinesis, reorganization of the interphase MF/MT cytoskeletons provides the structural basis for distinct distribution changes of ER-like membrane tubules and small vesicles, organelles which probably supply cell-wall precursor material (Fowke and Pickett-Heaps, 1969*b*; Grolig, 1990). Stage-specific effects of inhibitors revealed that the cytoskeletal rearrangements are an essential prerequisite for the coordinated progression of septum ingrowth and septum closure.

In stage 2, the extensive peripheral interphase actin cytoskeleton (Grolig, 1990) reorganizes into a circumferential MF array previously described by Goto and Ueda

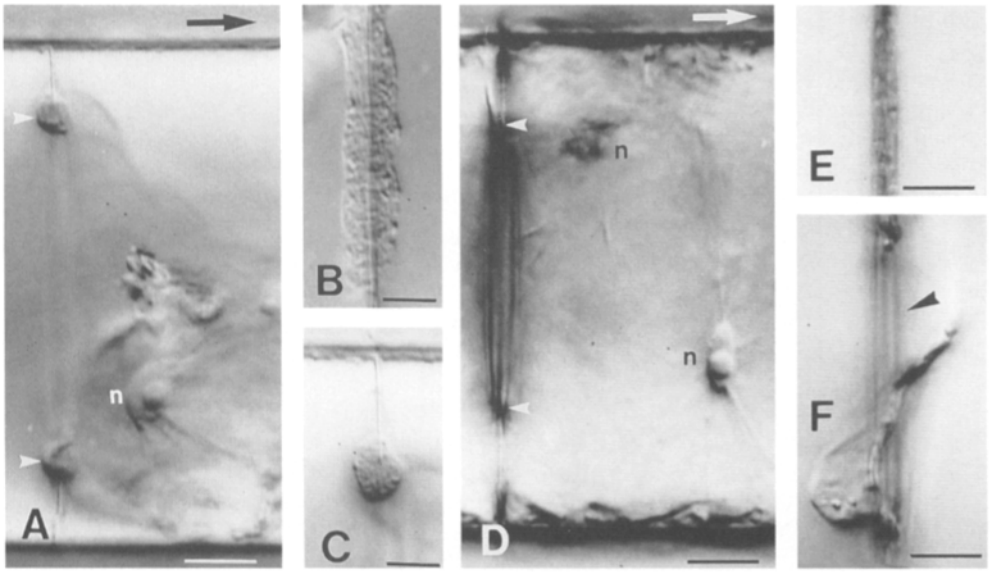

Figure 9. Live cells of *S. crassa*, centrifuged longitudinally for 20 min at 600 *g*. Long arrow indicates the direction of force. (*A–D*) Mitotic cells, which were centrifuged before formation of a basket structure. (*A–C*) Cell observed 30 min after centrifugation. (*A*) Midplane view shows the persistence of the organelle accumulation (*arrowheads*) at the edge of the septum indicating further ingrowth. Note the nucleus (*n*) with remnant interzonal strands of the diamond structure (*arrow*). (*B–C*) Same cell, details of the organelle accumulation. (*B*) Focus on septum edge showing organelle accumulation just as in untreated cells. (*C*) Midplane view reveals the radial arrangement of the organelles right at the septum edge. (*D*) Cell observed 4 d after centrifugation; midplane view. Premature termination of septum ingrowth (*arrowheads*) leaves a large gap in the centre. Both daughter nuclei (*n*, one is out of focal plane) reside in one half-cell. (*E–F*) Details of cytokinetic cells centrifuged after formation of the basket structure. (*E*) Focus on septum edge 2 h after centrifugation, a thin band of accumulated organelles indicates further ingrowth of the cross wall. (*F*) Midplane view 24 h after centrifugation. New cross wall almost completed, but with distortions in the direction of the ingrowth. A gap remains in the cross wall (*arrowhead*). Bars, 10 μm. In micrographs *A* and *D*, 20 μm.

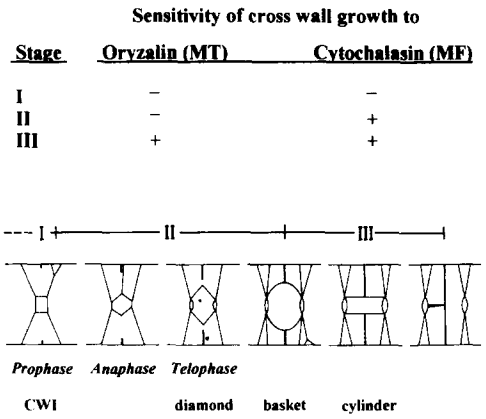

Figure 10. Three functional stages of cross wall growth can be discerned with respect to their susceptibility to cytoskeletal inhibitors. The sequence of these stages is related to characteristic structural changes during cytokinesis. Transition to MF-dependent growth occurs just after formation of the CWI, transition to MT-dependent growth during formation of the cylinder structure.

(1988). The MF bundles of this array aligned at various angles towards the CWI. Treatment at this stage with CD inhibited the progress of organelle accumulation towards the CWI. However, once the organelles had accumulated at the septum edge, the final accumulation could not be dissipated by CD. These findings suggest that organelles move along MF bundles towards the site of presumptive septum growth and are trapped there because of unidirectional and antiparallel alignment of the MFs (probably barbed end located at the septum edge).

In accordance with increased MT dynamics at the spindle poles, stiff cytoplasmic threads growing from the poles showed erratic growth and shrinkage. The susceptibility of these threads to oryzalin suggests that they include MTs of dynamic instability (Mitchison and Kirschner, 1984) which during the expansion of the diamond structure could provide a means to find the ingrowing septum in the cell periphery (Holy and Leibler, 1994). Such MTs finally seem to organize the basket structure, which is prerequisite for entering the third stage. Formation of the basket structure proceeded in the presence of CD (Fig. 8 *B*). Therefore, it does not depend on the presence of MFs, although MFs of the impinging septum seem to contribute to exact orientation of the basket in the cell.

At the beginning of stage 3, on transformation of the basket structure into the cylinder structure, application of oryzalin caused rapid breakdown of the MT scaffold and stopped septum ingrowth. Both in terms of genesis and MT arrangement, the cylinder structure corresponds to the phragmoplast-like structure described by Fowke and Pickett-Heaps (1969*b*). At this stage the actin array, focusing on the leading edge of the septum, no longer seems to be capable of supporting ingrowth on its own. The contact of the MT diamond with the growing edge of the septum altered the actin array: concomitant to transformation of the MT-organized diamond structure into the basket and then the cylinder structure, the septum-associated MFs became regularly oriented perpendicular to the plane of the septum. This was also reflected by a rearrangement of organelles (tubules and vesicles; cf. Fig. 2 *J* vs. 5 *G*). Translocation of such organelles towards the daughter nuclei increased along with the appearance of MF bundles extending from the daughter nuclei towards the septum edge.

Our centrifugation experiments indicate that in stage 3, the growing edge of the cross wall becomes more independent of the postmitotic structure consisting of the nuclei and the cytoplasmic cylinder between them: even though the growth direction was disturbed after centrifugation, in contrast to earlier stages, the growth process itself was not inhibited.

As transformation of the basket structure into the cylinder was abolished in the presence of CD and the basket structure disappeared, the association of MFs with MTs may contribute to the transformation of the thick MT bundles of the basket structure into the thinner bundles of the cylinder. When the basket structure has changed into the cylinder structure, MF bundles aligned along the MT(bundle)s and appeared to serve as tracks for draining off part of the organelle accumulation from the edge of the closing septum towards the daughter nuclei and from there, into the reestablishing interphase organelle translocation system of the NPS and the cell periphery. Because completion of septum ingrowth at stage 3 was affected by disruption of either MFs or MTs, the MT bundles of the cylindrical structure appear to serve as a template for reorganization of the septum-associated MF array. The cylindrical MT array apparently helps to overcome the, so far, rather uneven growth of the septum edge, possibly by promoting an even circumferential distribution of the septum-associated organelle accumulation after the chloroplasts have been severed. Despite this important supplementary function of the MTs, the translocation and accumulation of organelles remains actin based.

Early experiments by Van Wisselingh (1909) on a *Spirogyra* comparable in size to the one used in this study showed that dislocation of the mitotic apparatus by centrifugation did not impede further ingrowth of the septum, although the resulting cross walls were not straight (Fig. 9 *F*). The results of our centrifugation experiments with *S. crassa* differentiate and refine these observations: after centrifugation, the cross wall was completed (though nonperfectly) only if the basket structure had been in contact with the growing septum. However, if the mitotic apparatus of an earlier stage was displaced, ingrowth of the cross wall remained incomplete. This finding is consistent with the effects of oryzalin at early mitotic stages.

Cytokinesis in Spirogyra: Related to Higher Plant Cytokinesis?

All members of the Zygnemataceae investigated so far display an ingrowing septum finally impinging onto an open mitotic spindle which persists through telophase (Fowke and Pickett-Heaps, 1969*a*; Bech-Hansen and Fowke, 1972; Bakker and Lokhorst, 1987; Galway and Hardham, 1991). Another typical feature is that separation of chromosomes is accomplished by elongation of the spindle interzone (anaphase B), whereas anaphase A, movement of chromosomes to the poles, is minimal (Pickett-Heaps and Wetherbee, 1987). In principle, *S. crassa* shows the same mitotic features. Formation of a structure reminiscent of a phragmoplast has been described in two genera, *Spirogyra*

(Fowke and Pickett-Heaps, 1969*b*) and *Mougeotia* (Pickett-Heaps and Wetherbee, 1987). Fowke and Pickett-Heaps (1969*b*) suggested that this structure may represent an intermediate stage in the evolution of the phragmoplast found in recent higher plant cells.

The cytokinetic MT cytoskeleton in *Spirogyra* has functional aspects in common with the MT arrays seen in higher plant cell division, but also reveals pertinent differences. In both systems, MFs are intimately associated with the formation and development of the phragmoplast-like MT array. The higher plant phragmoplast is built by two circular, antiparallel arrays of MTs which interdigitate at their plus ends (Euteneuer et al., 1982) in the plane of the new cross wall. This array seems to be derived from preexisting interzone MTs by lateral coalescence (Zhang et al., 1993). In *S. crassa*, a similar MT array, perpendicular to the plane of cell division, is built by persisting interzonal MTs that contact the ingrowing septum. In cells of the advanced charophycean green alga *Coleochaete* (Brown et al., 1994) and in cells of higher plants the connection of the interzonal MTs to the daughter nuclei disappears, whereas the connection persists in *Spirogyra* (as in *Mougeotia* and *Zygnema*) until centripetal ingrowth has been completed. At least in higher plant cells additional MTs polymerize de novo at the circumference of the expanding phragmoplast (Vantard et al., 1990). In *S. crassa*, the observed increase in striation and improved perpendicular alignment during transformation of the basket structure into the cylinder suggests that some de novo polymerization of MTs occurs at the site of contact with the growing septum. This possibility is supported by the reported presence of electron-dense material, characteristic of microtubule organizing centers (Fowke and Pickett-Heaps, 1969*b*), and similar to that found in the higher plant phragmoplast. Alternatively, the observed reorganization might be elicited by the association with the massive MF array at the growing septum edge, mediated by MT-associated proteins that bind to MFs (Griffith and Pollard, 1978, 1982; Katsuta et al., 1990).

The MF cytoskeleton during cytokinesis in *Spirogyra* is distinct from the higher plant phragmoplast in several respects. First, cross wall growth in *Spirogyra* clearly depends on actin-based organelle translocation towards the growing edge. The MFs of the circumferential array at the growing edge of the cross wall then coalign with the MTs of the basket structure and, during transition to the phragmoplast-like structure, become oriented perpendicular to the cross wall plane, leading to a corresponding rearrangement of the septum-associated organelles. Our inhibitor experiments indicate that the interaction between MFs and MTs at this stage is indispensable for final success of cytokinesis. The pharmacological study of McIntosh et al. (1995), using the same inhibitors, found independently that the interaction between the septum and the expanded MT array is necessary for normal completion of the cross wall. Somewhat later, increased organelle translocation from the septum toward the nuclei occurs, probably after MFs of appropriate orientation have grown out from the reforming interphase NPS towards the septum, as indicated by increasing RLP fluorescence on the stalks of the NPS. In the higher plant phragmoplast, MFs are found parallel to the phragmoplast MTs, most filaments pointing with their barbed ends towards the developing cross wall (Kakimoto and Shibaoka, 1988). However, evidence from glycerinated (Asada et al., 1991) and from taxol-treated (Yasuhara et al., 1993) cells, as well as from proteins purified from isolated phragmoplasts (Asada and Shibaoka, 1994) suggests that phragmoplastic-vesicle transport in higher plants is driven by an ATP- or GTP-fueled, MT-associated mechanochemical enzyme. In contrast to the MTs, the phragmoplast MFs in higher plants appear to arise de novo from the proximal surface of the reforming nuclei, and they do not interdigitate within the midplane of the interzone (Zhang et al., 1993).

In higher plants, radial strands of F-actin have been reported to bridge the leading margin of the outgrowing phragmoplast to the opposing cortex, thereby presumably providing a "memory" of the predetermined division plane whose perimeter had been marked at preprophase by a band composed of microtubules and F-actin (Palevitz, 1987; Lloyd and Traas, 1988). No preprophase band was found in *S. crassa*, but cytoplasmic strands (Fig. 2 *D*) with fairly weak MF-related fluorescence (Fig. 3 *F*) radiate from the mitotic figure close to the area of the CWI. In addition, remnants of the interphase NPS persist at the spindle poles and continue to link the mitotic apparatus to the chloroplast bands in the peripheral cytoplasm. As mitosis proceeds unimpeded in the presence of CD, the MFs in the cytoplasmic strands (Fig. 3 *F*) appear to be less important than the residual MTs for keeping the mitotic apparatus in position. However, after contacting the diamond structure, the MFs of the ingrowing septum apparently contribute to proper orientation of this interzonal MT array (Fig. 8 *B*). In higher plants, cytochalasin impedes correct guidance of the edge of the growing phragmoplast to the division site previously marked by the cortical preprophase band (Mineyuki and Gunning, 1990).

Another difference appears in cell cycle–dependent reorganization of the cortical/peripheral arrays of MTs/MFs. While in higher plant cells, the cortical MF array at least partially remains throughout mitosis, the transverse cortical MT array disappears completely concomitant to formation of the preprophase band (Wick, 1991; Cleary et al., 1992). Inversely, in *Spirogyra* the extensive peripheral MF system of interphase disappears during formation of the cytokinetic array, while the cortical MTs diminish only gradually. The striking, local depletion of cortical MTs close to the ingrown cross wall (Fig. 4 *L*) as observed here towards the end of cytokinesis in *S. crassa* has not been described for any other zygnematacean species before. A comparable situation was described in higher plants (Cleary et al., 1992), although in this case MFs instead of MTs disappear adjacent to the new cross wall.

In summary, a phragmoplast precursor, rather than a real phragmoplast, occurs in *Spirogyra* and possibly those charophycean green algae, which divide by centripetal ingrowth of the cross wall. These cases probably include the zygnematacean algae, the desmids, the klebsormidiacaen algae, and the radial cell division of *Coleochaete*. The cell division of *Coleochaete*, cell plate growth for circumferential division, and cross wall ingrowth for radial division (Marchant and Pickett-Heaps, 1973; Brown et al., 1994), seem to represent an intermediate stage between lower (centripetally dividing) and higher (centrifugally dividing,

e.g., *Chara* and *Nitella*) charophycean algae. Further work on the structure and function of the cytokinetic MF and MT cytoskeleton is needed to reveal further common ground and the differences of the cytokinetic arrays within the group of centripetally dividing Charophyceae.

We are indebted to Dr. Julia Willingale-Theune (Max-Planck-Institut [MPI] für Zellbiologie, Ladenburg, FRG) for helpful suggestions to improve the manuscript and to Drs. Diedrik Menzel (MPI für Zellbiologie) and Albert Duschl (Biozentrum, Würzburg, FRG) for critical reading of the manuscript. We thank Drs. Goeffrey O. Wasteneys, Diedrik Menzel, and Mike Savage (MPI für Zellbiologie) for their help at the confocal scanning microscope, and Professor Jeremy Pickett-Heaps (School of Botany, Melbourne, Australia) for communicating information not yet published. We gratefully acknowledge a generous gift of rhodamine phalloidin from Professor Theodor Wieland (MPI für medizinische Forschung, Heidelberg, FRG), and thank Andrea Weisert and Joachim Döring for technical assistance during preparation of the manuscript, and Heiko Häuser for video support.

This work was supported by the Deutsche Forschungsgemeinschaft (Gr 910-1).

Received for publication 26 January 1995 and in revised form 11 May 1995.

References

Asada, T., and H. Shibaoka. 1994. Isolation of polypeptides with microtubule-translocating activity from phragmoplasts of tobacco BY-2 cells. *J. Cell Sci.* 107:2249–2257.

Asada, T., S. Sonobe, and H. Shibaoka. 1991. Microtubule translocation in the cytokinetic apparatus of cultured tobacco cells. *Nature (Lond.).* 350:238–241.

Bakker, M. E., and G. M. Lokhorst. 1987. Ultrastructure of mitosis and cytokinesis in *Zygnema sp.* (Zygnematales, Chlorophyta). *Protoplasma.* 138:105–118.

Baskin, T. I., and W. Z. Cande. 1990. The structure and function of the mitotic spindle in flowering plants. *Annu. Rev. Plant Physiol. Plant Mol. Biol.* 41: 277–315.

Bech-Hansen, C. W., and L. C. Fowke. 1972. Mitosis in *Mougeotia sp. Can. J. Bot.* 50:1811–1816.

Brown, R. C., B. E. Lemmon, and L. E. Graham. 1994. Morphogenetic plastid migration and microtubule arrays in mitosis and cytokinesis in the green alga *Coleochaete orbicularis. Am. J. Bot.* 81:127–133.

Cleary, A. L., B. E. S. Gunning, G. O. Wasteneys, and P. K. Hepler. 1992. Microtubule and F-actin dynamics at the division site in living *Tradescantia* stamen hair cells. *J. Cell Sci.* 103:977–988.

De Jesus, M. D., F. Tabatabai, and D. J. Chapman. 1989. Taxonomic distribution of copper–zinc superoxide dismutase in green algae and its phylogenetic importance. *J. Phycol.* 25:767–772.

Devereux, R., A. R. Loeblich, and G. F. Fox. 1990. Higher plant origins and the phylogeny of green algae. *J. Mol. Evol.* 31:18–24.

Euteneuer, U., W. T. Jackson, and J. R. McIntosh. 1982. Polarity of spindle microtubules in *Haemanthus* endosperm. *J. Cell Biol.* 94:644–653.

Fowke, L. C., and J. D. Pickett-Heaps. 1969*a*. Cell division in *Spirogyra.* I. Mitosis. *J. Phycol.* 5:240–259.

Fowke, L. C., and J. D. Pickett-Heaps. 1969*b*. Cell division in *Spirogyra.* II. Cytokinesis. *J. Phycol.* 5:273–281.

Fujii, S., T. Shimmen, and M. Tazawa. 1978. Light-induced changes in membrane potential in *Spirogyra. Plant Cell Physiol.* 19:573–590.

Galway, M. E., and A. R. Hardham. 1991. Immunofluorescent localization of microtubules throughout the cell cycle in the green alga *Mougeotia* (Zygnemataceae). *Am. J. Bot.* 78:451–461.

Goto, Y., and K. Ueda. 1988. Microfilament bundles of F-actin in *Spirogyra* observed by fluorescence microscopy. *Planta (Heidelb.).* 173:442–446.

Graham, L. E., C. F. Delwiche, and B. D. Mishler. 1991. Phylogenetic connections between the 'Green algae' and the 'Bryophytes.' *Adv. Bryol.* 4:213–244.

Griffith, L. M., and T. D. Pollard. 1978. Evidence for actin filament–microtubule interaction mediated by microtubule-associated proteins. *J. Cell Biol.* 78:958–965.

Griffith, L. M., and T. D. Pollard. 1982. The interaction of actin filaments with microtubules and microtubule-associated proteins. *J. Biol. Chem.* 257:9143–9151.

Grolig, F. 1990. Actin-based organelle movements in interphase *Spirogyra. Protoplasma.* 155:29–42.

Grolig, F. 1992. The cytoskeleton of the *Zygnemataceae. In* The Cytoskeleton of the Algae. D. Menzel, editor. CRC Press Inc., Boca Raton, FL. 165–194.

Grolig, F., R. E. Williamson, J. Parke, C. Miller, and B. H. Anderton. 1988. Myosin and Ca^{2+}-sensitive streaming in the alga *Chara*: detection of two polypeptides reacting with a monoclonal anti-myosin and their localization in the streaming endoplasm. *Eur. J. Cell Biol.* 47:22–31.

Gunning, B. E. S. 1982. The cytokinetic apparatus: its development and spatial regulation. *In* The Cytoskeleton in Plant Growth and Development. C. W. Lloyd, editor. Academic Press Inc., New York. 229–295.

Holy, T. E., and S. Leibler. 1994. Dynamic instability of microtubules as an efficient way to search in space. *Proc. Natl. Acad. Sci. USA.* 91:5682–5685.

Hoshaw, R. W., and R. M. McCourt. 1988. The *Zygnemataceae* (Chlorophyta): A twenty-year update of research. *Phycologia.* 27:511–548.

Kakimoto, T., and H. Shibaoka. 1988. Cytoskeletal ultrastructure of phragmoplast-nuclei complexes isolated from cultured tobacco cells. *Protoplasma Suppl.* 2:95–103.

Katsuta, J., Y. Hashiguchi, and H. Shibaoka. 1990. The role of the cytoskeleton in positioning of the nucleus in premitotic tobacco BY-2 cells. *J. Cell Sci.* 95: 413–422.

Lloyd, C. W., and J. A. Traas. 1988. The role of F-actin in determining the division plane of carrot suspension cells: drug studies. *Development (Camb.).* 102:211–221.

Marchant, H. J., and J. D. Pickett-Heaps. 1973. Mitosis and cytokinesis in *Coleochaete scutata. J. Phycol.* 9:461–471.

Mattox, K. R., and K. D. Stewart. 1984. Classification of the green algae: a concept based on comparative cytology. *In* Systematics of the Green Algae. D. E. G. Irvine and D. M. John, editors. Academic Press Ltd., London. 29–72.

McIntosh, K., J. D. Pickett-Heaps, and B. E. S. Gunning. 1995. Cytokinesis in *Spirogyra*: integration of cleavage and cell-plate formation. *Int. J. Plant Sci.* 156:1–8.

Mineyuki, Y., and B. E. S. Gunning. 1990. A role for the preprophase band of microtubules in maturation of new cell walls, and a general proposal on the function of preprophase band sites in cell division of higher plants. *J. Cell Sci.* 97:527–537.

Mitchison, T., and M. Kirschner. 1984. Dynamic instability of microtubule growth. *Nature (Lond.).* 312:237–242.

Morejohn, L. C., T. E. Bureau, J. Molé-Bajer, A. S. Bajer, and D. E. Fosket. 1987. Oryzalin, a dinitronaniline herbicide, binds to plant tubulin and inhibits microtubule polymerization in vitro. *Planta (Heidelb.).* 172:252–264.

Palevitz, B. A. 1987. Actin in the preprophase band of *Allium cepa. J. Cell Biol.* 104:1515–1519.

Pickett-Heaps, J. D. 1975. Green Algae. Sinauer Associates Inc., Sunderland, MA.

Pickett-Heaps, J. D., and H. J. Marchant. 1972. The phylogeny of the green algae: a new proposal. *Cytobios.* 6:255–264.

Pickett-Heaps, J. D., and R. Wetherbee. 1987. Spindle function in the green alga *Mougeotia*: absence of anaphase A correlates with postmitotic nuclear migration. *Cell Motil. Cytoskeleton.* 7:68–77.

Schliwa, M. 1982. Action of cytochalasin D on cytoskeletal networks. *J. Cell Biol.* 92:79–91.

Surek, B., U. Beemelmanns, M. Melkonian, and D. Bhattacharya. 1994. Ribosomal RNA sequence comparisons demonstrate an evolutionary relationship between *Zygnematales* and charophytes. *Plant Syst. Evol.* 191:171–181.

Staiger, S. J., and C. W. Lloyd. 1991. The plant cytoskeleton. *Curr. Opin. Cell Biol.* 3:33–42.

Van Wisselingh, C. 1909. Zur Physiologie der *Spirogyra*zelle. *Beih. Bot. Centralblatt.* 12:133–210.

Vantard, M., N. Levilliers, A. M. Hill, A. Adoutte, and A. M. Lambert. 1990. Incorporation of *Paramecium* axonemal tubulin into higher plant cells reveals functional sites of microtubule assembly. *Proc. Natl. Acad. Sci. USA.* 87:8825–8829.

Warburg, O., and G. Krippahl. 1960. Weiterentwicklung der manometrischen Methoden (Carbonatgemische). *Z. Naturforsch. Sect. B Chem. Sci.* 15:364–367.

Waris, H. 1953. The significance for algae of chelating substances in the nutrient solution. *Physiol. Plant.* 6:538–543.

Wick, S. M. 1991. Spatial aspects of cytokinesis in plant cells. *Curr. Opin. Cell Biol.* 3:253–260.

Yasuhara, H., S. Sonobe, and H. Shibaoka. 1993. Effects of taxol on the development of the cell plate and of the phragmoplast in tobacco BY-2 cells. *Plant Cell Physiol.* 34:21–29.

Zhang, D., P. Wadsworth, and P. K. Hepler. 1993. Dynamics of microfilaments are similar, but distinct from microtubules during cytokinesis in living, dividing plant cells. *Cell Motil. Cytoskeleton.* 24:151–155.